Biomaterials 117 (2017) 44–53

Contents lists available at ScienceDirect

Biomaterials

journal homepage: www.elsevier.com/locate/biomaterials

Antigen recognition-triggered drug delivery mediated by nanocapsule-functionalized cytotoxic T-cells

R. Brad Jones [a, b, c], Stephanie Mueller [a, c], Sudha Kumari [a, c], Vlad Vrbanac [a, d], Shy Genel [e], Andrew M. Tager [a], Todd M. Allen [a], Bruce D. Walker [a, f, g, h], Darrell J. Irvine [a, c, g, h, i, *]

[a] Ragon Institute of MGH, MIT, and Harvard, Cambridge, MA, USA
[b] Dept of Microbiology, Immunology, and Tropical Medicine, The George Washington University, Washington DC, USA
[c] Koch Institute for Integrative Cancer Research, MIT, Cambridge, MA, USA
[d] Center for Immunology and Inflammatory Diseases, MGH, Boston, MA, USA
[e] Astronomy Dept., Columbia University, New York, NY, USA
[f] Dept. of Microbiology and Immunology, Harvard Medical School, Boston, MA, USA
[g] Dept. of Biological Engineering, MIT, Cambridge, MA, USA
[h] Dept. of Materials Science & Engineering, MIT, Cambridge, MA, USA
[i] Howard Hughes Medical Institute, Chevy Chase, MD, USA

ARTICLE INFO

Article history:
Received 13 September 2016
Received in revised form
20 November 2016
Accepted 24 November 2016
Available online 25 November 2016

Keywords:
Drug delivery
Cytotoxic T lymphocytes
Lipid nanocapsules
Immunotherapy
T-pharmacyte

ABSTRACT

Cytotoxic T-Lymphocytes (CTLs) kill pathogen-infected or transformed cells following interaction of their T-cell receptors (TCRs) with foreign (e.g. virus-derived) peptides bound to MHC-I molecules on the target cell. TCR binding triggers CTLs to secrete perforin, which forms pores in the target cell membrane, promoting target death. Here, we show that by conjugating drug-loaded lipid nanoparticles to the surface of CTLs, their lytic machinery can be co-opted to lyse the cell-bound drug carrier, providing triggered release of drug cargo upon target cell recognition. Protein encapsulated in T-cell-bound nanoparticles was released following culture of CTLs with target cells in an antigen dose- and perforin-dependent manner and coincided with target cell lysis. Using this approach, we demonstrate the capacity of HIV-specific CTLs to deliver an immunotherapeutic agent to an anatomical site of viral replication. This strategy provides a novel means to couple drug delivery to the action of therapeutic cells *in vivo*.

1. Introduction

The ability to precisely control the spatial and temporal delivery of therapeutic agents *in vivo* would revolutionize the treatment of human disease. This overarching goal has motivated the development of stimuli-responsive nanoparticles designed to release drug cargos in response to the chemical properties of a target tissue environment, such as the low pH of tumors; or in response to physical stimuli such as light, heat, or magnetic fields applied to an anatomical target site (reviewed in Refs. [1,2]). A promising strategy is to interface drug delivery technologies with cell therapy, by conjugating or loading therapeutic cells with drug delivery payloads [3–10] (reviewed in Ref. [11]). In such approaches, programmed or environment-responsive drug release provided by a synthetic drug carrier can be married with the precision tissue homing properties of living cells. We previously demonstrated that cytotoxic T-lymphocytes (CTLs) can carry drug-loaded nanoparticles through the covalent attachment of lipid-based nanocapsules to cell surface proteins [6,7,11,12]. These nanocapsule-CTL conjugates (NC-CTL) exhibited unimpaired abilities to kill target cells and trafficked normally *in vivo*, accumulating in tumors that expressed cognate antigen [6,7,11,12]. In this work we used NC-CTL technology to focus drug delivery on the CTLs themselves, through a pseudo-autocrine mechanism [6], or to deliver drugs to tumors by passive release [7]. However, it would be attractive to control the timing and location of drug payload release by linking it to cell function, and in the case of therapeutic T-cells, to link drug delivery to antigen recognition – which would localize payload release to sites of antigen expression (e.g., infected tissues or tumors) and avoid premature drug release at other sites like blood and lymphoid tissues.

* Corresponding author. Ragon Institute of MGH, MIT, and Harvard, Cambridge, MA, USA.
E-mail address: djirvine@mit.edu (D.J. Irvine).

http://dx.doi.org/10.1016/j.biomaterials.2016.11.048
0142-9612/

Here we demonstrate that one of the key functions of cytotoxic lymphocytes, lytic granule exocytosis, can be used as a trigger to release therapeutic payloads from CTL-bound nanoparticles. We show that, as CTLs recognize antigen displayed on the surface of target cells, lipid-based nanoparticles chemically conjugated to the surface of these cells are trafficked to the T-cell/target cell contact site (the immunological synapse). Subsequent release of the membrane pore-forming protein perforin at the synapse leads to both disruption of the target cell membrane and the membrane of the lipid drug carrier, leading to rapid cargo release (Fig. 1). In an *in vivo* model of HIV infection, we demonstrate that HIV-specific CTLs carrying nanoparticles loaded with an immunotherapeutic agent (the interleukin IL-15), can specifically release this cytokine in tissues where infected cells are detected, resulting in enhanced elimination of infected cells as compared to HIV-specific CTLs with empty nanoparticles. This approach provides a general platform for achieving time- and space-regulated drug delivery, by linking drug release to the highly sensitive and specific sensing of antigens by CTLs.

2. Materials and methods

2.1. Ethics statement

HIV-infected individuals were recruited from the Maple Leaf Medical Clinic in Toronto, Canada through a protocol approved by the University of Toronto Institutional Review Board. Secondary use of the samples from Toronto was approved through the Massachusetts General Hospital (MGH) Institutional Review Board. All subjects were adults, and gave written informed consent. Animal experiments were performed under a protocol approved by the MGH and MIT IACUCs.

2.2. Generation of T-cell clones

Peripheral blood mononuclear cells (PBMCs). were stimulated with optimal CD8 T-cell epitopes for 6-h, enriched for antigen-specific cells using the IFN-γ secretion Detection and Enrichment Kit (Miltenyi), and cloned at limiting dilution on irradiated feeder cells as has been previously described [13]. Clones were selected from 96-well plates at dilutions where no more than 1 in 5 wells displayed growth and screened for specificity by IFN-γ ELISPOT. Specific clones were expanded on irradiated feeder cells.

2.3. Generation of ICMV nanocapsules

ICMVs were generated as previously described. Briefly, 0.1 mg of DOPG 0.4 mg of DOPC and 0.65 mg of maleimide containing lipid MPB were combined in chloroform and dried to lipid films (lipids from Avanti Polar Lipids). These films were resuspended in a buffer of 20 mM Bis-tris propane pH 7.2 containing 10.0 mg/ml Alexa647-OVA (Life Technologies), or 0.7 mg/ml of the IL-15Sa ALT-803 (Altor Bioscience Corporation), by multiple rounds of vortexing. Mixtures were sonicated for 5 min to form unilamellar nanoparticles and then $CaCl_2$ was added to induce the fusion of particles into multilamellar structures. Particles were then crosslinked by treating with DTT, resulting in the formation of covalent bonds between maleimide functional groups in neighboring lipid bilayers. Particles were then pelleted, washed twice with water, and resuspended in XVIVO-10 serum-free medium (Lonza). IL-15Sa encapsulation was determined by lysing particles and performing enzyme linked immunosorbent assay (ELISA), and calculated as 2.46 ± 0.10 μg of IL-15Sa per 1.15 mg of lipid (0.21%).

2.4. Generation of NC-CTLs

CTL clones were used 2–3 weeks after the most recent restimulation with irradiated feeder cells. A full batch of ICMVs as described above was combined with 50×10^6 CTLs and incubated at 37 °C for 1 h with constant agitation. Cells were then pelleted at 1200 × g for 5 min, washed twice with 1 ml each of XVIVO-10 medium, and resuspended in 200 μL of 10 mg/ml polyethylene glycol thiol (PEG-SH) in PBS for 10 min at 37 °C to quench free maleimide groups. Resulting NC-CTLs were then resuspended in RPMI +10% FBS + penicillin/streptomycin + L-glutamine (R-10) supplemented with 50 U/ml IL-2 (Hofmann La Roche) (R10-50), and used in downstream applications. For the cells used in the *in vivo* experiment depicted in Fig. 5, IL-15Sa cargo loading was calculated as 216 ± 4 ng/10^6 NC-CTLs by lysis and ELISA.

2.5. Assessing NC-CTL polarization

Alexa-647 OVA NC-CTLs were co-cultured with peptide-pulsed CFSE-labeled autologous $CD4^+$ T cells (targets) for 20 min at 37 °C. Cells were then fixed with 2% paraformaldehyde (PFA), stained with Phalloidin Alexa-658 and DAPI in 0.005% Triton-X100 for two hours, and imaged by confocal microscopy. Maximum intensity projects were generated for 56 conjugate images. For each

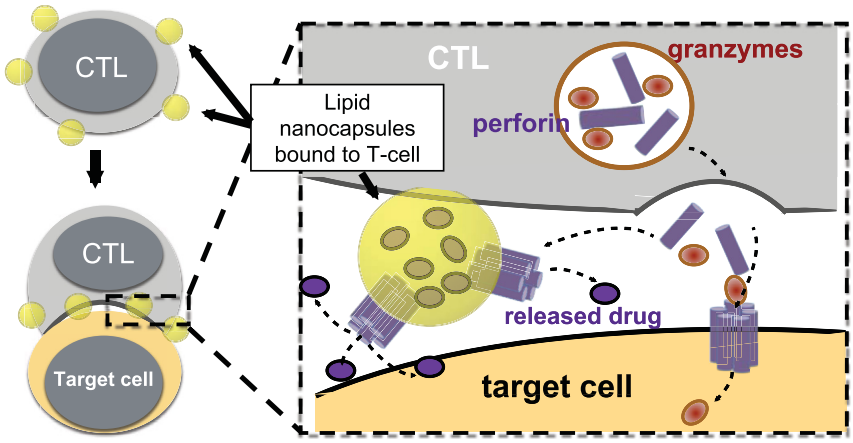

Fig. 1. Strategy for CTL-triggered drug release from lipid nanocapsules. CTLs encountering target cells release perforin and granzymes into the immunological synapse formed between the CTL and target cell. Lipid nanocapsules (NCs) covalently anchored to CTL surface proteins traffic into the synapse, where they are exposed to perforin released by the CTL, enabling disruption of the NC and release of encapsulated drug in tandem with lysis of the target cell.

of these images, lines were drawn parallel to synaptic planes, through the middles of NC-CTLs. NC-CTLs were defined as having polarized NCs into synapse with target cells if >50% of Alexa-647 OVA intensity was above this line (towards target).

2.6. Testing ability of recombinant perforin to disrupt ICMVs

An amount of ICMVs comprising ~0.23 mg of lipid (one fifth of a batch as described above) that had been loaded with 10 mg/ml of Alexa647-OVA were resuspended in 250 μL of buffer (150 mM NaCl, 1 mM $CaCl_2$, 20 mM HEPES in ddH_2O, pH 7.2). ICMVs were aliquoted into wells of a V-bottom 96-well plate at 25 μL/well. Recombinant perforin (Abcam) was received at 942 nM, diluted to 100 nM and 10-fold serially diluted down to 0.1 nM in the above buffer. These perforin solutions were then added to pelleted BLCL (1×10^6 cells/well) or to ICMVs. Samples were mixed and incubated at 37 °C for 2 h, then pelleted, resuspended in XVIVO-10 medium and incubated for an additional 14 h at 37 °C. On the following day, cells/ICMVs were pelleted, supernatants were transferred to black 96-well plates, and fluorescence was quantified at 647 absorbance and 694 emission.

2.7. Assessing triggered release from TCR-Stimulated NC-CTLs

NC-CTLs loaded with Alexa647-OVA were co-cultured for 3–16 h (as indicated in figure legends) with anti-CD3/anti-CD28 Dynabeads (Thermo Fisher Scientific) at the indicated NC-CTL:beads ratios; or with an excess of BLCLs matched on the restricting MHC-I allele and pulse/washed with cognate peptide. Co-cultures were performed in R10-50 medium at 37 °C. In some experiments supernatants were retained to quantify released cargo by ELISA. Cells were then stained with fluorochrome-conjugated Abs to CD3 and CD8 (Biolegend). Cargo release was assessed by flow cytometry, gating on $CD3^+CD8^+$ lymphocytes and assessing cell-associated cargo by Alexa647 fluorescence. In some experiments, we simultaneously assessed degranulation (CD107a exposure) by adding anti-CD107a PE (Biolegend) at the beginning of the co-culture period. Note that Brefeldin A was not used in these experiments. To test the effects of the perforin inhibitor concanamycin A (CMA) on triggered release, NC-CTLs were co-cultured with the indicated concentrations of CMA (Sigma) for 3 h, washed three times, then tested in triggered release assays as above.

2.8. Time lapse microscopy of triggered release from NC-CTLs

NC-CTLs and peptide-pulsed target cells were generated as above. 3D collagen matrix time-lapse microscopy was performed as previously described [14]. Sytox Green Nuleic Acid Stain (Thermo Fisher Scientific) was incorporated into the matrix gel at a final concentration of 5 μM to allow for visualization of killed cells.

2.9. Image analysis of time lapse microscopy

The deviation from Gaussian pixel intensity distribution was calculated in two steps. First, the full pixel distributions were fit to a Gaussian curve using the linear least-squares method. Second, the absolute values of the differences between the best-fit and the actual distributions were summed across all pixel intensity values and the result was divided by the total number of pixels. The result represents the fractional area of the image that contributes to a non-Gaussian pixel intensity distribution. All calculations were performed in MATLAB (MathWorks).

2.10. Assessing triggered release In vivo

NSG mice were reconstituted with $CD4^+$ T-cells from an HLA-$A02^+$ HIV-uninfected donor by tail vein injection of 1×10^7 cells. Engraftment was allowed to proceed until day 35, when absolute $CD4^+$ T-cell counts in the blood were >250 cells/mm^3 as assessed by flow cytometry using CountBright Absolute Counting Beads (Thermo Fisher Scientific). Mice were then either infected with 10,000 $TCID_{50}$/mouse of the CXCR4-tropic HIV molecular clone LAI by IP injection (10 mice), or injected with an equal volume of PBS (uninfected controls, 5 mice). Infections were allowed to proceed for 8 days, at which point HIV viral loads exceed 1×10^6 copies/ml for all infected animals. Mice were then injected by tail vein with 2.5×10^6/mouse NC-CTLs specific for the HLA-A02-restricted HIV-Gag FLGKIWPSYK epitope. The 5 uninfected mice and one group of 5 infected mice received NC-CTLs that had been loaded with 0.7 mg/ml of IL-15Sa. The other group of 5 infected mice received empty NC-CTLs. Two days later, mice were euthanized. Cervical and axillary lymph nodes were pooled for a given animal and disrupted to single cell suspensions in 0.5 ml PBS. The IL-15Sa in these samples was then quantified by ELISA using the R&D Systems Human IL-15 Immunoassay, following the manufacturer's instructions. Estimated lymph node concentrations were calculated based on a 3 mm^3 lymph node volume [15,16]. Cells were stained with fluorochrome-conjugated antibodies to human CD45, mouse CD45, human CD3, human CD4, and human CD8 (all from Biolegend), then fixed and permeabilized using the BD cytofix/cytoperm system following the manufacturer's instructions, and then stained intracellularly with PE-conjugated anti-HIV-Gag antibody (Kc57 clone, Beckman Coulter). Cells were then analyzed by flow cytometry.

3. Results

3.1. The lytic granule effector perforin lyses crosslinked lipid nanocapsules

On binding of the TCR to cognate peptide-MHC complexes on the surface of target cells, CTLs exocytose lytic granules, polymeric complexes of multiple proteins involved in target cell lysis. A key component is perforin, a 67 KDa protein that self-assembles in cell membranes to promote delivery of apoptosis-inducing granzyme proteins into the target cell [17]. Perforin can also permeabilize simple single-bilayer synthetic liposomes, where it forms 19-24-membered protein channels 50–300 Å in diameter [18]. However, liposomes exhibit a low efficiency for encapsulation of macromolecular drugs, and we thus instead employed interbilayer-crosslinked multilamellar vesicles (ICMVs) as a drug carrier. These multilamellar crosslinked lipid capsules [referred to hereafter as nanocapsules (NCs)] encapsulate proteins much more efficiently than traditional liposomes [19,20]. We first tested whether recombinant perforin could disrupt the integrity of multilamellar NCs, resulting in the release of encapsulated cargo.

We prepared NCs loaded with Alexa Fluor 647-conjugated Ovalbumin (Alexa647-OVA) as a model protein cargo. Lipid films containing anionic phosphatidyl glycerol lipids and maleimide-headgroup lipids were rehydrated in the presence of the labeled protein, induced to fuse via the addition of calcium, and the capsule walls were crosslinked by low concentrations of dithiothreitol (DTT) as reported previously [19] (Fig. 2A). The resulting OVA-loaded NCs were incubated in buffer with or without addition of 1 nM perforin, which in preliminary experiments was shown to lead to nearly complete lysis of a human B lymphoblastoid cell line (data not shown), followed by fluorescence measurements to quantify the fraction of Alexa647-OVA released into the

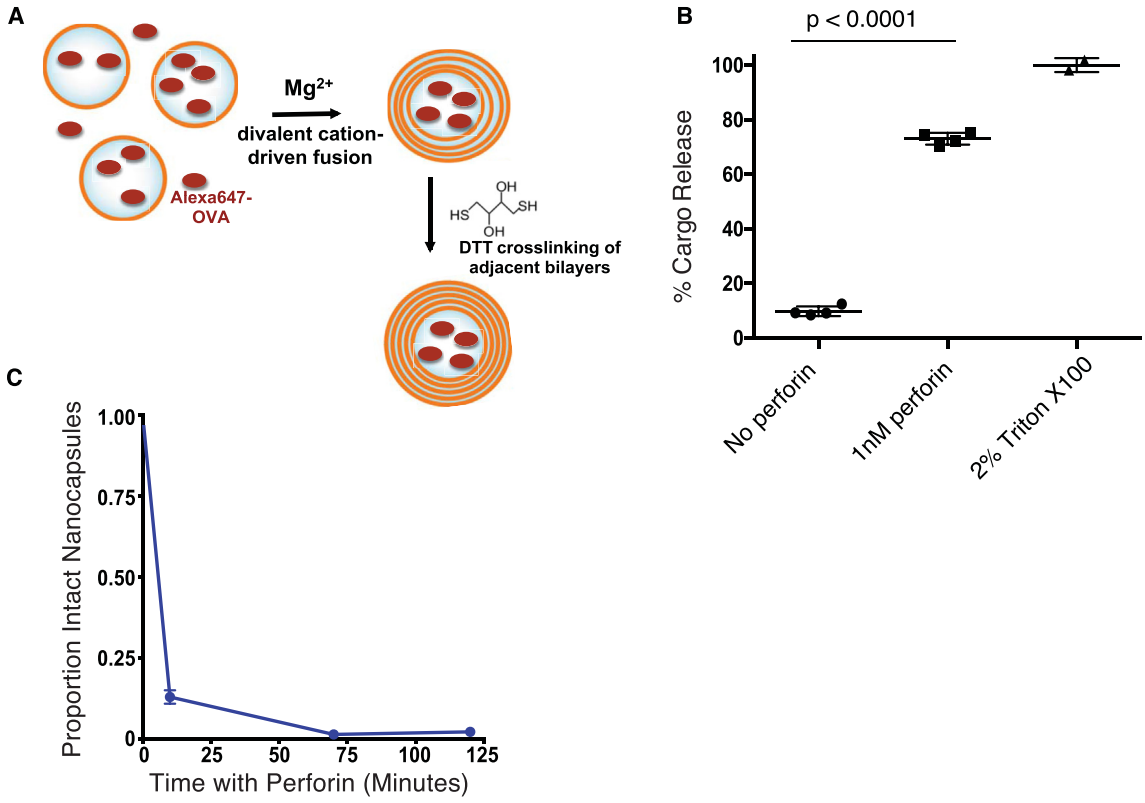

Fig. 2. Perforin can rupture synthetic lipid nanocapsules to release encapsulated protein cargos. A. Schematic of ICMV lipid nanocapsule (NC) synthesis. **B**. Alexa647-OVA-loaded lipid NCs were incubated with 1 nM perforin, buffer only control, or 2% Triton-X100 for 8 h at 37 °C. Particles were pelleted by centrifugation, and OVA protein released into the supernatants was quantified by fluorescence measurements. Values are expressed as % cargo release relative to the mean of the Triton X-100 controls (100%). Means ± SEM are depicted and the *p* value was calculated by ANOVA with Holm-Sidak's multiple comparison test. **C**. Alexa647-OVA-loaded lipid NCs were incubated with 1 nM perforin. Intact NCs were quantified relative to an internal control by flow cytometry, and are expressed relative to the t = 0 sample.

supernatant. Following incubation for 8 h at 37 °C, ~73% of Alexa647-OVA was released from NCs incubated with perforin, approaching the positive control of NCs lysed by the detergent 2% Triton-X100 ($p < 0.0001$, Fig. 2B). By contrast, almost no protein was released from particles incubated without perforin (Fig. 2B). Thus, low concentrations of perforin were sufficient to rapidly trigger the release of protein cargo from ICMV nanocapsules.

We next used flow cytometric analysis of particles to assess the kinetics of perforin-mediated cargo release. This approach also allowed us to determine whether cargo was released through pores formed in intact NCs, which would manifest as diminution of Alexa-647, or through the rupture of NCs, and thus the loss of detectable particles. We observed that particles were ruptured rapidly, with an 87% ± 14% reduction in intact particles by the first time-point, 10 min after the addition of perforin (Fig. 2C).

3.2. NC-CTLs triggered through the TCR release nanocapsule-carried protein in a perforin-dependent manner

The ability of perforin to disrupt NCs made it plausible that CTL recognition of antigens could trigger release of cargo if NCs are localized in the immunological synapse. Thus, we next examined the cell surface distribution of nanocapsules conjugated to human CTLs during target cell recognition. CTLs engaging antigen-bearing target cells traffic many cell surface receptors into the CTL/target contact site (the immunological synapse) [21]. We previously showed that maleimide-mediated conjugation of nanocapsules to free thiols on cell surface proteins of mouse T-cells coupled the particles to several receptors (e.g., CD45, LFA-1, and Thy1) known to polarize to the synapse during T-cell recognition [12]. During T-cell engagement of tumor cells, the particles were found to be carried by these anchoring receptors into the synapse [12]. To determine if similar synapse localization of particles occurs with human CTLs, maleimide-functionalized NCs loaded with Alexa647-OVA were conjugated to the surface of a human CTL clone specific for the HIV Gag-FLGKIPSYK epitope. Nanocapsule-conjugated CTLs (NC-CTLs) in suspension showed NCs dispersed randomly over the cell surface, as we previously observed for mouse T-cells (Fig. 3A – top right). However, when NC-CTLs were mixed with antigen-bearing target $CD4^+$ cells in co-culture for 20 min, then fixed and imaged, we found that 55% of the total CTL/target bicellular conjugates had polarized their capsule cargo to the cell interface (see Methods), mirroring what we had previously seen for mouse T-cells engaging tumor cells (Fig. 3A – bottom row). A 3D reconstruction of the conjugate in the right panel of Fig. 3A is given in Supplementary Movie 1.

Supplementary video related to this article can be found at http://dx.doi.org/10.1016/j.biomaterials.2016.11.048.

We next evaluated whether cell-bound NCs would be disrupted to release cargo following triggering of the CTL's TCR, using flow cytometry to detect loss of CTL-associated cargo protein fluorescence following T-cell activation with anti-CD3-coated beads (Fig. 3B). CTLs specific for the pp65 antigen of human cytomegalovirus (CMV) were conjugated with OVA-loaded NCs and then stimulated with anti-CD3/CD28 beads for 16 h, followed by flow cytometry analysis to detect cell-associated Alexa647-OVA and surface CD3 levels. Unstimulated NC-CTLs cultured for 16 h were predominantly $CD3^{hi}$ and had high levels of associated Alexa647-

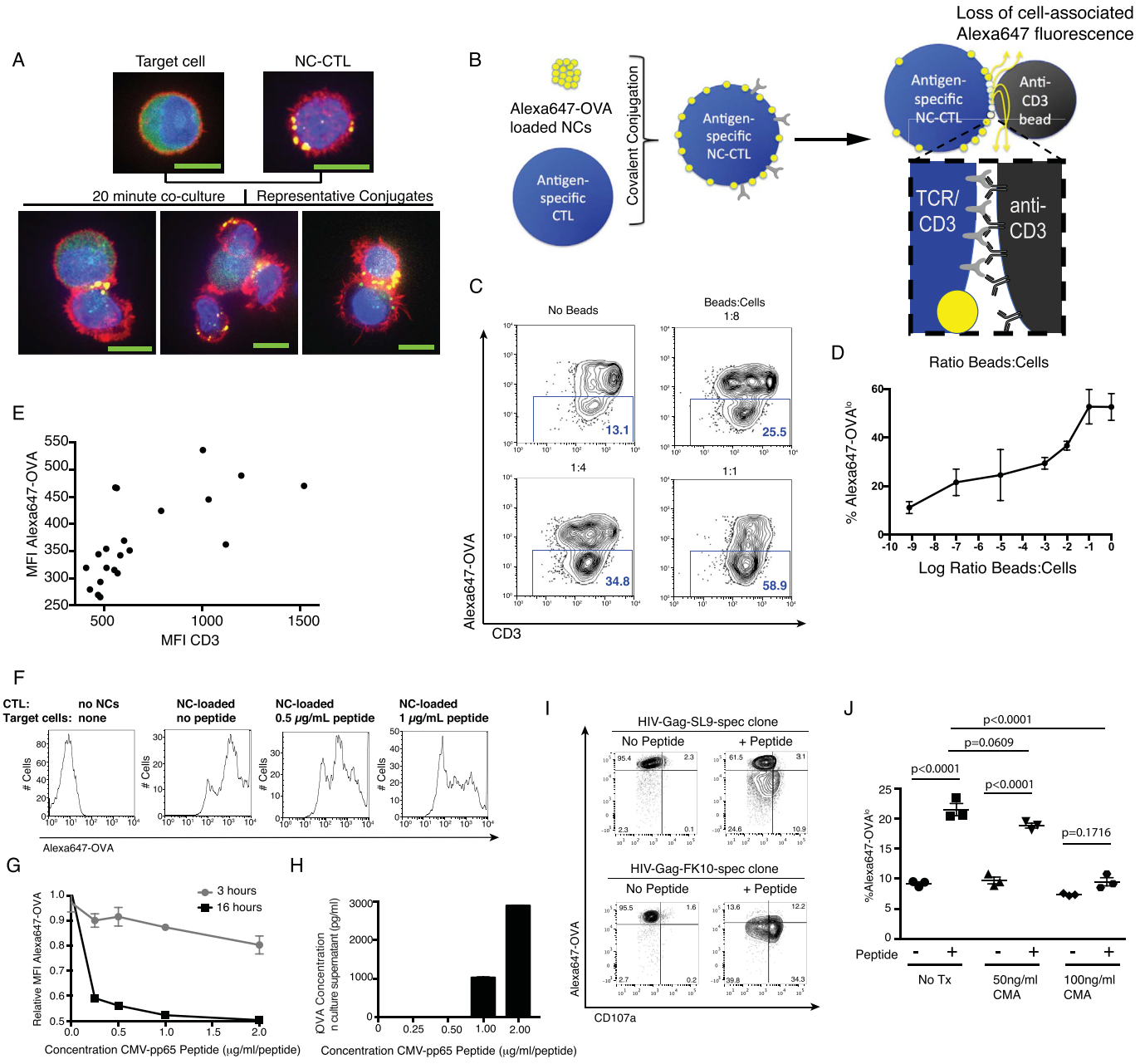

Fig. 3. T-cell receptor stimulation triggers release of contents from T-cell conjugated lipid nanocapsules. A. NC-conjugated CTLs were mixed with CFSE-labeled target cells for 20 min, then fixed and stained for microscopy. Shown are confocal images depicting NCs distributed over the cell surface of an isolated NC-CTL (top right) and concentrated into the immunological synapse with target cells (lower panels). Yellow = Alexa-647 OVA NCs, Green = CFSE-labeled targets, blue = DAPI, red = actin (Phalloidin Alexa-658). Scale bar, 10 μM. **B**. Schematic of experimental setup to detect TCR triggered release. **C-E**. CMV-specific CTLs conjugated with Alexa647-OVA-loaded NCs were stimulated with anti-CD3 beads for 16 h and then analyzed by flow cytometry. Shown are representative flow cytometry plots depicting CD3 and Alexa647-OVA levels on NC-CTLs at the indicated bead:cell ratios (**C**), summary means ± SEM of triplicate samples (**D**), and a graph of the MFI of Alexa647-OVA vs. CD3 from each individual sample condition analyzed in **D** (**E**). **F**–**H**. NC-CTLs were prepared as in **C** and stimulated with autologous BLCL target cells pulsed with cognate CMV peptide. Following 3 or 16 h of co-culture, cells were analyzed by flow cytometry. Shown are histograms indicating progressive losses in CTL-associated OVA fluorescence with increasing concentrations of peptide (**F**), mean ± SEM from triplicate samples (**G**), and ELISA data measuring Alexa647-OVA concentrations in cell culture supernatants from the same experiment following 12 h of co-culture (**H,** showing mean ± SEM from duplicate samples). Alexa647-OVA fluorescence in G is normalized to the starting signal at time zero. **I**. An HIV-Gag SL9 specific T-cell clone and an HIV-Gag FK10 specific T-cell clone were conjugated with Alexa647-OVA loaded NCs, then co-cultured with HLA-A02^{+} CD4^{+} T-cells that had been pulsed with cognate peptide or (or left unpulsed as controls). Shown are flow cytometry data after 16 h co-culture depicting relative Alexa647-OVA and CD107a levels. **J**. HIV-Gag SL9-specific CD8^{+} T-cell clones were treated with the perforin inhibitor Concanamycin A (CMA) or with vehicle control ('No Tx') for 3 h, conjugated with Alexa647-OVA-loaded NCs, then co-cultured for 16 h with autologous BLCL that had either been pulsed with SL9 peptide or maintained as unpulsed controls. Shown are summary flow cytometry data presenting percentages of Alexa647-OVA dim cells (gated as in **C**). P values were calculated by ANOVA.

OVA fluorescence, indicating low levels of spontaneous release of the encapsulated protein cargo from the cell-bound particles (Fig. 3C and D). By contrast, with increasing bead:T-cell ratios we observed the progressive emergence of a population of Alexa647-OVA^{lo} cells with an MFI ~10× lower than the OVA fluorescence of unstimulated cells, suggesting lysis of cell-bound particles and release of Alexa647-OVA (Fig. 3C and D). As T-cells are activated through the TCR/CD3 complex, both TCRs and the associated

signaling protein CD3 are internalized, with the degree of internalization correlating with the strength of TCR triggering [22]. Using the same samples as in Fig. 3C and D, we observed that the loss of surface levels of CD3 correlated with reductions in the amounts of NC-CTL cargo at a population level. This correlation is consistent with TCR triggering, induced by the addition of anti-CD3 beads, driving the release of NC cargo (Fig. 3E).

To assess if engagement of the TCR with natural peptide-MHC ligands presented by target cells would trigger release of cell-bound cargo, CMV-specific NC-CTLs were co-cultured with target cells [autologous B lymphoblastoid cells (BLCLs) pulsed with cognate peptide] for 3 or 16 h, then analyzed by flow cytometry. The stimulation of NC-CTLs with target cells bearing increasing concentrations of peptide antigen was associated with the progressive loss of cell-associated Alexa647-OVA that increased with time, again indicative of TCR stimulation triggering cargo release (Fig. 3F and G). In parallel, we measured Alexa647-OVA in supernatants of the cultures by ELISA, and found that Alexa647-OVA levels correlated with the peptide pulsing concentration of the target cells (Fig. 3H). Thus, triggering of NC-CTLs led to antigen level-dependent release of nanocapsule-encapsulated cargo.

If antigen recognition-associated Alexa647-OVA release is mediated by perforin from the triggered CTLs, it should be limited to cells that degranulated (the exocytotic mechanism of perforin release). CTLs that degranulate in response to antigen transiently expose the lytic granule-associated protein CD107a on their surface, allowing for labeling with a fluorescently-labeled antibody. Using two different HIV Gag-specific Alexa647-OVA-loaded NC-CTLs, targeting SLYNTVATL 'SL9' or FLGKIWPSYK 'FK10' peptide determinants, we observed that NC-CTLs that lost Alexa647-OVA fluorescence were the same cells that had encountered a target cell and degranulated (Fig. 3I). We note that substantially greater levels of both degranulation and of cargo release were observed with the FK10-specific as compared to the SL9-specific NC-CTLs. HIV-specific CTLs are well known to be functionally heterogeneous and to have differential abilities to kill HIV-infected and peptide pulsed cells [23]. Thus, we speculate that the degree of cargo release that occurs following an encounter with an antigen-presenting target cells may also be tunable by virtue of the cytotoxic capacity of the selected CTL.

To determine whether Alexa647-OVA release was mediated by perforin, we employed an inhibitor of perforin-based cytotoxic activity, concanamycin A (CMA), which acts by accelerating the degradation of perforin within lytic granules [24]. The HIV-Gag SL9-specific CTL clone was treated with 0, 50, or 100 ng/ml of CMA for 3 h, conjugated with Alexa647-OVA-loaded nanocapsules, and then co-cultured with autologous SL9-pulsed target cells. Approximately 23% of control NC-CTLs not exposed to CMA showed a loss of cell-associated Alexa647-OVA following culture with target cells, while NC-CTLs treated with 50 ng/ml of CMA exhibited a trend toward reduced Alexa647-OVA release ($p = 0.0609$) and NC-CTLs treated with 100 ng/mL CMA exhibited almost complete abrogation of triggered release ($p < 0.0001$, Fig. 3J. Thus, TCR-stimulated triggered release of cargo from NC-CTLs is perforin-dependent.

3.3. Release of protein cargo from cell-bound nanocapsules coincides with engagement and killing of target cells

Following TCR triggering, perforin release begins within 30 min and continues for at least 120 min. [25], but the overall kinetics of nanocapsule rupture in our experiments also reflects the time required for a given T-cell to locate and engage a target cells, which can require hours [14]. Our flow cytometry measurements indicated that release of cell-bound protein cargo is detectable within a few hours, and progresses for at least 16 h; this could reflect either a slow release process on the single-cell level, or a distribution of times needed for CTLs to engage target cells in the co-cultures. To determine the temporal dynamics between release of perforin from CTLs and the release of cell-bound OVA at the single cell level, we utilized time-lapse microscopy of T-cells and target cells in collagen matrices to visualize triggered release of cargo from NC-CTLs. CMV-specific NC-CTLs carrying Alexa647-OVA were mixed with control or peptide-pulsed target cells in collagen, in the presence of the reporter dye sytox, which fluoresces brightly on binding to DNA of lysed cells [14]. As we previously reported [12], particle-decorated T-cells migrating through the collagen matrix polarized their membrane-bound nanocapsule cargo to the uropod (tail) (Fig. 4A, time 0:01, and Supplementary Movie 2). Time-lapse imaging revealed that as NC-CTLs engaged target cells, lysis of peptide-pulsed target cells was rapidly followed by the dispersion of Alexa647-OVA cargo around the kill site (Fig. 4A, Supplementary Movie 2). No such cargo release was observed when these NC-CTLs were co-cultured with target cells lacking the cognate peptide (Fig. 4B, Supplementary Movie 3). An additional example of lysis-triggered cargo release from an NC-CTL is shown in Supplementary Fig. 1, this time using an HIV-Gag-specific CTL clone.

Supplementary video related to this article can be found at http://dx.doi.org/10.1016/j.biomaterials.2016.11.048.

In the event depicted in Fig. 4A, NC-CTL cargo was released into the immediate surroundings following CTL killing of a target cell, consistent with perforin-mediated NC disruption. This is captured by the kymograph in Fig. 4C depicting the evolution of signal along a single vertical line drawn through the center of the target/CTL conjugates (red arrow in Fig. 4A), and plotting the sytox and OVA signal fluorescence signals along this line over time, showing the spread of OVA signal away from the conjugate site over time. To further characterize the relationship between the kinetics of triggered protein release and engagement/killing of target cells in these time-lapse microscopy experiments, we carried out an analysis of the intensity distribution of fluorescent OVA cargo protein and the sytox cell viability reporter dye from many fields of view. The pixel intensity in the Alexa647 channel (all pixels in a field of view) exhibited a Gaussian distribution at baseline, with the exception of a small minority of pixels representing the Alexa647-OVA-loaded nanoparticles, which fell between this peak and saturation. In control cultures lacking antigen, this Gaussian distribution was maintained, with a modest progressive shift towards higher mean pixel intensities likely representing a small amount of spontaneous Alexa647-OVA-protein release from nanocapsules in the absence of T-cell lytic activity (Fig. 4D). In contrast, in the peptide-pulsed conditions, the Alexa647-OVA overall fluorescence intensity distribution both showed a greater shift towards higher pixel intensities, and a deviation from a Gaussian distribution as OVA protein was enriched in the proximity of target cell kill-sites (Fig. 4D). Plotting the deviation from a Gaussian distribution for the intensity data as a function of time (see Methods) thus provided a means for quantitative tracking of the overall kinetics of cargo release. Cargo release in the peptide-pulsed condition was preceded by target cell perforation as measured by total Sytox fluorescence in the fields of view (Fig. 4E and F), and was significantly greater than in the no peptide control ($p = 0.0286$, Fig. 4G). Thus, these videomicroscopy analyses suggest that NC-CTLs release their bound cargo locally at the site of antigen engagement over a period of a few hours following target cell engagement and delivery of a lethal hit. These finding suggest the delayed release of cargo observed in the experiments of Fig. 3 likely reflect delayed times for CTLs to engage targets in the previous co-culture experiments (which notably were carried out in the absence of a migration-supporting collagen matrix).

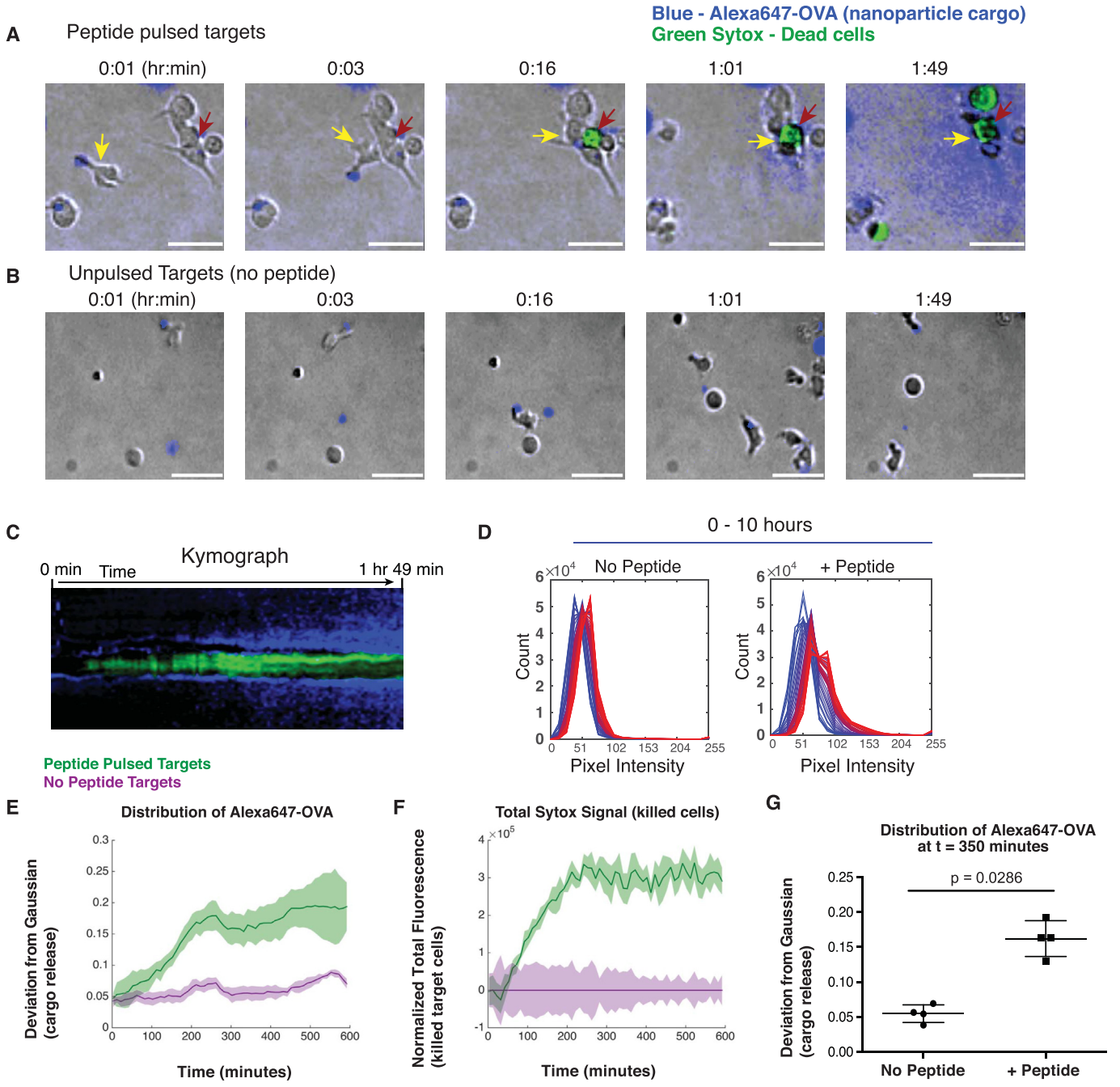

Fig. 4. Release of NC-CTL cargo coincides with CTL engagement and lysis of target cells. CMV-specific CTLs were conjugated with Alexa647-OVA-loaded NCs, then introduced with peptide-pulsed autologous BLCL target cells or unpulsed control BLCL into a collagen matrix and imaged by videomicroscopy. **A**. Timelapse frames illustrating example migrating NC-CTL (yellow arrows, OVA-loaded NCs (blue) visible at the tail of the cell) engaging a target cell (red arrow) at t = 3 min. Target cell lysis occurs at 16 min (sytox green fluorescence) followed over the next 1.5 h by dispersal of Alexa647-OVA fluorescence (blue) from the multiple CTLs engaged on the target cell. Scale bar = 15 μM. **B**. NC-CTLs (yellow arrows) in control wells where target cells are not bearing cognate antigen migrate without killing target cells and Alexa647-OVA is not appreciably released. **C**. Kymograph centered around the kill site shown in **A** (red arrow) depicting relative timing of target cell killing (sytox, green) and OVA dispersal (blue). **D**. Histograms show the distributions of pixel intensities in the Alexa647 channel at various times for no peptide (left panel) and + peptide (right panel) conditions. The 50 histograms in each panel span 10 h of evolution, sampled every 12 min, going from blue to red with time. The shifts towards the right in the no peptide histograms represent baseline release of Alexa647-OVA by diffusion or particle degradation. The more pronounced shits towards the right in the + peptide histograms provide evidence of more rapid release triggered by peptide recognition. **E**. Quantification of Alexa647-OVA signal deviation from Gaussian distribution. The absolute values of the differences between the Gaussian best-fits and the actual distributions (**D**) were summed across all pixel intensity values and the result was divided by the total number of pixels. Mean ± SD values are shown from four fields of view (FOV) each for peptide-pulsed targets (green) and no peptide targets (purple). **F**. Quantification of mean ± st.dev. sytox signal vs. time (averaged from 4 FOV for peptide-pulsed targets (blue) and no peptide targets (red)). Signals for both conditions were normalized by subtraction of total Sytox fluorescence in the no peptide conditions as a function of time. **G**. A Mann-Whitney test was applied to determine whether the distribution of Alexa647 OVA (cargo release) was significantly different between −peptide and +peptide wells at T = 350 min [after killing had plateaued (**F**)].

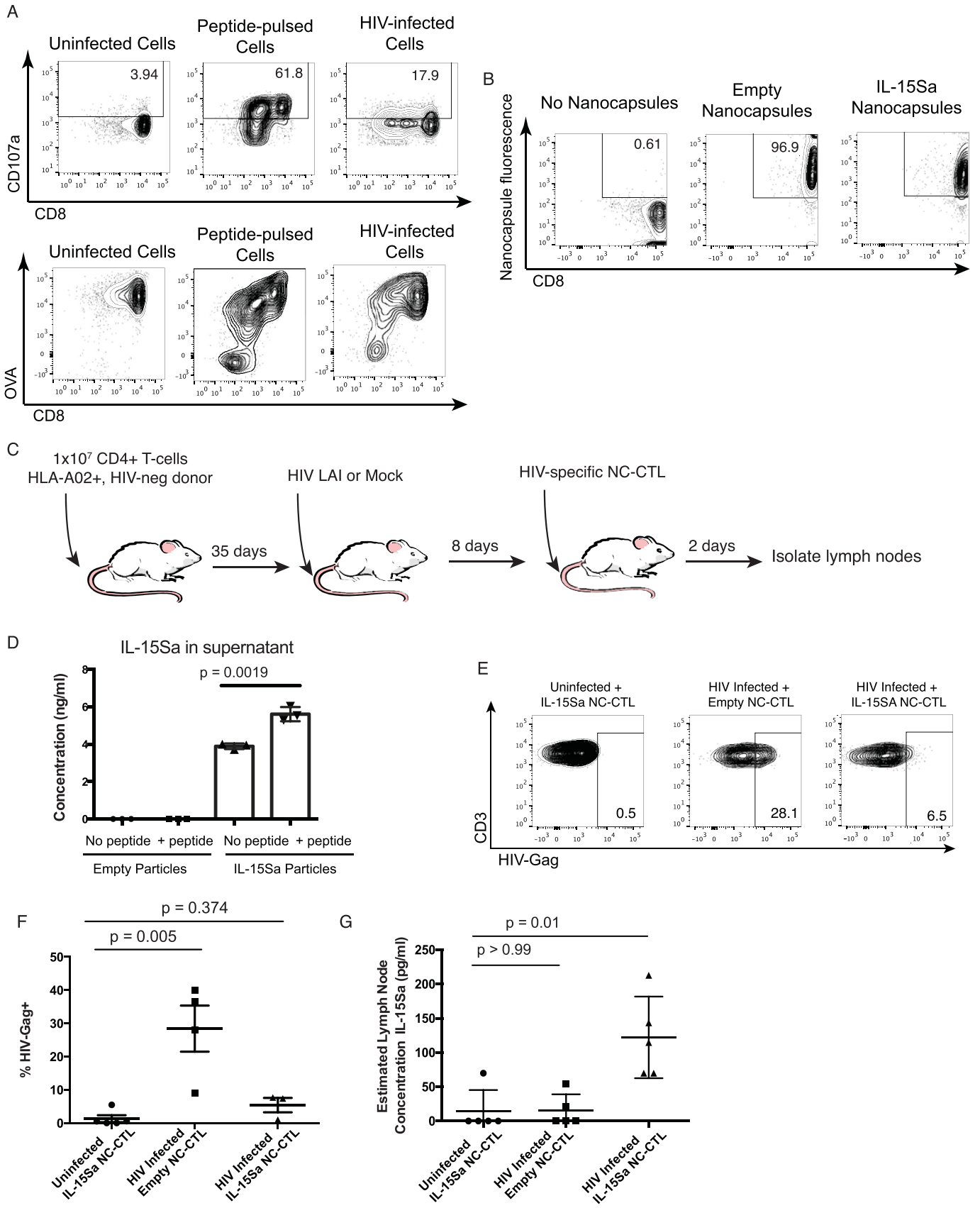

Fig. 5. Antigen recognition triggers release of NC-T-cell cargo *in vivo*. A & B. HIV gag FK10-specific CTLs were conjugated with either Alexa647-OVA-loaded or IL-15Sa-loaded nanocapsules for *in vitro* analysis. **A**. Alexa647-OVA loaded NC-CTLs were co-cultured with HLA-A02$^+$ CD4$^+$ T-cells (same donor as used for *in vivo* experiments) that had either been infected with HIV-LAI (right panels), mock infected and pulsed with the FK10 peptide (middle panels), or left uninfected and unpulsed (negative controls, left panel). Shown are flow

3.4. HIV-specific NC-CTLs release therapeutic proteins in response to infected cell recognition in vivo

To test whether antigen-triggered drug release can occur *in vivo* and to illustrate the potential utility of this approach for therapeutic purposes, we utilized a humanized mouse model of HIV infection. Adoptive transfer of HIV-specific CTLs into HIV-infected individuals has been proposed as a strategy to eradicate HIV reservoirs that persist in antiretroviral therapy (ART)-treated individuals [26,27], but such approaches may require both a means of enhancing the function of HIV-specific CTLs, and of inducing HIV antigen expression from latent reservoirs using a latency reversing agent (LRA) [28,29]. We recently discovered that an IL-15 superagonist (IL-15Sa, a complex of the immunocytokine IL-15 with a soluble form of the IL-15 receptor α chain) is able to enhance CTL recognition of infected target cells [30]. In addition, we previously demonstrated that IL-15Sa "backpacked" on T-cells could significantly enhance CTL proliferation and function in a model of tumor immunotherapy [6]. We hypothesized that IL-15Sa-carrying NC-T-cells encountering target cells would simultaneously exhibit enhanced survival/function *in vivo* and dose the surrounding tissue with the cytokine. Here we took a first step toward this ultimate goal by testing whether NC-T-cells carrying IL-15Sa would exhibit enhanced recognition/killing of target cells *in vivo*, and assayed for antigen-triggered cytokine release in tissues.

We first evaluated whether NC-T-cells would exhibit triggered release in response to physiological antigen presentation from HIV-infected target cells *in vitro*. CTLs specific for the HIV-Gag peptide were loaded with Alexa647-OVA-carrying NCs and mixed with peptide-pulsed, mock infected, or HIV-infected autologous primary $CD4^+$ T-cells as targets. As shown in Fig. 5A (upper panel), NC-T-cells degranulated, expressing surface CD107a in co-cultures containing infected target cells or peptide-pulsed target cells but not mock-infected controls. In addition, NC-CTLs lost cell-associated Alexa647-OVA in co-cultures with HIV-infected targets, indicating antigen recognition-triggered NC lysis (Fig. 5A, lower panel).

Next, we prepared IL-15Sa-loaded nanocapsules, which released IL-15Sa over >7 days *in vitro* (Supplementary Fig. 2) or empty nanocapsules controls. These nanocapsules were conjugated to HIV-Gag-specific T-cells at indistinguishable levels from each other (Fig. 5B), achieving a cytokine loading of 216 ± 4 ng IL-15Sa per 10^6 T-cells for the loaded particles. Immunodeficient NOD-scid $IL2R\gamma^{-/-}$ (NSG) mice were reconstituted with $CD4^+$ T-cells from an $HLA\text{-}A02^+$ HIV-negative donor, and then either infected with HIV, or maintained as uninfected controls. Eight days after viral inoculation, when HIV viral loads in infected mice were $>1 \times 10^6$ copies/ml, mice were injected with IL-15Sa-carrying or control (empty particle) NC-T-cells (Schematic - Fig. 5C). Since 2.5×10^6 NC-T-Cells were injected per mouse, the total dose of IL-15Sa was 540 ng/mouse. In parallel, a portion of the same NC-T-cells were placed in co-culture *in vitro* with autologous $CD4^+$ target cells that were pulsed with the target antigen or kept antigen-free as controls. ELISA measurements on the supernatants of the *in vitro* co-cultures at 18 h revealed that the NC-T-cells carrying IL-15Sa selectively released substantial quantities into the culture in a manner dependent on the recognition of peptide-pulsed target cells (Fig. 5D). *In vivo*, we observed superior antiviral function of IL-15Sa-loaded versus empty particle control NC-T-cells, as evidenced by a lower frequency of HIV-infected (Gag^+) $CD4^+$ T-cells recovered from the lymph nodes of mice that received the cytokine-carrying CTLs (Fig. 5E and F). In parallel, we observed significantly greater amounts of IL-15Sa in the extracellular fluid of lymph nodes taken from HIV-infected versus uninfected mice, supporting the triggered release of this cargo following recognition of HIV antigens (Fig. 5G). Note that we did not observe preferential accumulation of NC-CTLs in the lymph nodes of HIV-infected versus uninfected lymph nodes (means of 6.5×10^4 versus 5.4×10^4 CTLs, respectively). Thus, the release of NC-CTL cargo can be triggered by *in vivo* recognition of antigens. In the case of HIV infection, IL-15Sa-loaded NC-CTLs exhibited superior antiviral function.

4. Conclusions

Cytotoxic T-lymphocytes possess the machinery to recognize an almost unlimited diversity of antigens with exquisite specificity, and release lytic proteins following sensing of as few as ~3–10 molecules [31]. Here we have demonstrated the ability to harness this machinery to achieve antigen-triggered release of cell-bound nanoparticle drug cargos. This approach offers the opportunity to guide nanoparticle delivery *in vivo* by manipulating the migration patterns of CTLs, coupled with context-specific release of drugs in response to detection of disease-associated antigens in tissues (e.g. viral or tumor antigens). CTL-mediated triggered release could be readily applied to chimeric antigen receptor (CAR) T cells, which express an antibody or other engineered binding protein instead of a natural TCR [32], providing a means to link drug release to the detection of specific target molecules in tissues. A limitation of this strategy is the potential of T cells to release a majority of their associated drug cargo in response to a single target recognition event. However, this is balanced by the potential of NC-CTLs to both specifically accumulate drug carriers in target tissues and provide context-specific drug release with high fidelity, two long-standing major goals in drug delivery. Altogether, this approach provides a powerful strategy for combining immunotherapy and targeted drug delivery applicable to both cancer and infectious disease.

One potential application of IL-15Sa-loaded NC-T-cells that we would highlight is the potential utility as a therapeutic approach to purging the HIV reservoirs that persist in individuals on antiretroviral (ARV) therapy. In addition to enhancing the antiviral function of CTLs, IL-15Sa is able to induce the expression of HIV antigens from latently-infected cells, previously invisible to CTL recognition [30]. These cells form a stable HIV reservoir in the lymphoid tissue of ARV-treated individuals [33–35]. Thus, in the current study we have demonstrated the ability to specifically deliver a latency-reversing agent to an important anatomical reservoir. In future work we will test the potential of this means of coordinating targeted latency reversal with effective CTLs to reduce latent viral reservoirs.

cytometry data of the CTLs after 16 h depicting CD107a and CD8 expression (upper panels) and Alexa647-OVA vs. CD8 expression (lower panels). **B**. Levels of DiD-labeled empty or IL-15Sa-loaded NCs conjugated to FK10-specific CTLs were analyzed by flow cytometry. **C**. Experimental plan of adoptive cell therapy study using NC-CTLs to treat HIV-infected humanized mice. **D**. A fraction of IL-15Sa-loaded HIV-specific NC-CTLs prepared for the adoptive transfer *in vivo* study were in parallel cultured with peptide-pulsed or unpulsed autologous $CD4^+$ T-cells for 18 h, and IL-15SA released into the supernatants was measured by ELISA. **E-G**. HIV-infected or uninfected humanized mice were injected with FK10-specific NC-CTLs, where NCs were empty or loaded with IL-15Sa. Shown are representative flow cytometry data on lymphocytes harvested from lymph nodes gated on human T-cells ($huCD45^+CD3^+$) 2 days after T cell transfer (**E**), summary mean ± SEM percentages of infected cells in lymph nodes (**F**), and IL-15Sa present in lymph nodes quantified by ELISA (**G**). Estimated lymph node concentrations were calculated based on a 3 mm^3 lymph node volume [15,16]. Shown are means ± SEM. P values were calculated by Kruskal-Wallis with Dunn's multiple comparison test. Cells were not detected by flow cytometry in one of the samples from the HIV-infected empty NC-CTL mice, and two of the HIV infected IL-15Sa NC-CTL mice (**F**) – the latter of which corresponds with the two lowest IL-15Sa concentrations in **G**.

Acknowledgments

This work was supported by the Ragon Institute of MGH, MIT, and Harvard, and the NIH (AI111860). DJI and BDW are Investigators of the Howard Hughes Medical Institute. We gratefully acknowledge Hing Wong and Emily Jeng of Altor Bioscience Corporation for helpful discussion and for provision of ALT-803. RBJ is a Junior Investigator of the Ontario HIV Treatment Network and a Canadian Institutes of Health Research Banting Fellow.

Appendix A. Supplementary data

Supplementary data related to this article can be found at http://dx.doi.org/10.1016/j.biomaterials.2016.11.048.

References

[1] R. Lehner, X. Wang, S. Marsch, P. Hunziker, Intelligent nanomaterials for medicine: carrier platforms and targeting strategies in the context of clinical application, Nanomedicine 9 (2013) 742–757.
[2] S. Mura, J. Nicolas, P. Couvreur, Stimuli-responsive nanocarriers for drug delivery, Nat. Mater. 12 (2013) 991–1003.
[3] M.R. Choi, K.J. Stanton-Maxey, J.K. Stanley, C.S. Levin, R. Bardhan, D. Akin, et al., A cellular Trojan Horse for delivery of therapeutic nanoparticles into tumors, Nano Lett. 7 (2007) 3759–3765.
[4] H. Dou, C.B. Grotepas, J.M. McMillan, C.J. Destache, M. Chaubal, J. Werling, et al., Macrophage delivery of nanoformulated antiretroviral drug to the brain in a murine model of neuroAIDS, J. Immunol. 183 (2009) 661–669.
[5] J. Murciano, S. Medinilla, D. Eslin, E. Atochina, D. Cines, V. Muzykantov, Prophylactic fibrinolysis through selective dissolution of nascent clots by tPA-carrying erythrocytes, Nat. Biotechnol. 21 (2003) 891–896.
[6] M.T. Stephan, J.J. Moon, S.H. Um, A. Bershteyn, D.J. Irvine, Therapeutic cell engineering with surface-conjugated synthetic nanoparticles, Nat. Med. 16 (2010) 1035–1041.
[7] B. Huang, W.D. Abraham, Y. Zheng, S.C. Bustamante Lopez, S.S. Luo, D.J. Irvine, Active targeting of chemotherapy to disseminated tumors using nanoparticle-carrying T cells, Sci. Transl. Med. 7 (2015) 291ra94.
[8] Y. Zheng, M.T. Stephan, S.A. Gai, W. Abraham, A. Shearer, D.J. Irvine, In vivo targeting of adoptively transferred T-cells with antibody- and cytokine-conjugated liposomes, J. Control Release 172 (2013) 426–435.
[9] J.A. Ankrum, O.R. Miranda, K.S. Ng, D. Sarkar, C. Xu, J.M. Karp, Engineering cells with intracellular agent-loaded microparticles to control cell phenotype, Nat. Protoc. 9 (2014) 233–245.
[10] K. Schnarr, R. Mooney, Y. Weng, D. Zhao, E. Garcia, B. Armstrong, et al., Gold nanoparticle-loaded neural stem cells for photothermal ablation of cancer, Adv. Healthc. Mater. 2 (2013) 976–982.
[11] M.T. Stephan, D.J. Irvine, Enhancing cell therapies from the outside in: cell surface engineering using synthetic nanomaterials, Nano Today 6 (2011) 309–325.
[12] M.T. Stephan, S.B. Stephan, P. Bak, J. Chen, D.J. Irvine, Synapse-directed delivery of immunomodulators using T-cell-conjugated nanoparticles, Biomaterials 33 (2012) 5776–5787.
[13] R.B. Jones, F.Y. Yue, X.X. Gu, D.V. Hunter, S. Mujib, G. Gyenes, et al., Human immunodeficiency virus type 1 escapes from interleukin-2-producing CD4+ T-cell responses without high-frequency fixation of mutations, J. Virol. 83 (2009) 8722–8732.
[14] M.H. Foley, T. Forcier, E. McAndrew, M. Gonzalez, H. Chen, B. Juelg, et al., High avidity CD8+ T cells efficiently eliminate motile HIV-infected targets and execute a locally focused program of anti-viral function, PLoS One 9 (2014) e87873.
[15] S.T. Proulx, E. Kwok, Z. You, M.O. Papuga, C.A. Beck, D.J. Shealy, et al., Longitudinal assessment of synovial, lymph node, and bone volumes in inflammatory arthritis in mice by in vivo magnetic resonance imaging and microfocal computed tomography, Arthritis Rheum. 56 (2007) 4024–4037.
[16] F. Yang, C. Jin, D. Yang, Y. Jiang, J. Li, Y. Di, et al., Magnetic functionalised carbon nanotubes as drug vehicles for cancer lymph node metastasis treatment, Eur. J. Cancer 47 (2011) 1873–1882.
[17] I. Voskoboinik, J.C. Whisstock, J.A. Trapani, Perforin and granzymes: function, dysfunction and human pathology, Nat. Rev. Immunol. 15 (2015) 388–400.
[18] R.H. Law, N. Lukoyanova, I. Voskoboinik, T.T. Caradoc-Davies, K. Baran, M.A. Dunstone, et al., The structural basis for membrane binding and pore formation by lymphocyte perforin, Nature 468 (2010) 447–451.
[19] J.J. Moon, H. Suh, A. Bershteyn, M.T. Stephan, H. Liu, B. Huang, et al., Interbilayer-crosslinked multilamellar vesicles as synthetic vaccines for potent humoral and cellular immune responses, Nat. Mater. 10 (2011) 243–251.
[20] J.J. Moon, H. Suh, A.V. Li, C.F. Ockenhouse, A. Yadava, D.J. Irvine, Enhancing humoral responses to a malaria antigen with nanoparticle vaccines that expand Tfh cells and promote germinal center induction, Proc. Natl. Acad. Sci. U. S. A. 109 (2012) 1080–1085.
[21] P. Anton van der Merwe, S.J. Davis, A.S. Shaw, M.L. Dustin, Cytoskeletal polarization and redistribution of cell-surface molecules during T cell antigen recognition, Semin. Immunol. 12 (2000) 5–21.
[22] S. Valitutti, S. Muller, M. Salio, A. Lanzavecchia, Degradation of T cell receptor (TCR)-CD3-zeta complexes after antigenic stimulation, J. Exp. Med. 185 (1997) 1859–1864.
[23] S.A. Migueles, D. Mendoza, M.G. Zimmerman, K.M. Martins, S.A. Toulmin, E.P. Kelly, et al., CD8(+) t-cell cytotoxic capacity associated with human immunodeficiency Virus-1 control can be mediated through various epitopes and human leukocyte antigen types, EBioMedicine 2 (2015) 46–58.
[24] T. Kataoka, N. Shinohara, H. Takayama, K. Takaku, S. Kondo, S. Yonehara, et al., Concanamycin A, a powerful tool for characterization and estimation of contribution of perforin- and Fas-based lytic pathways in cell-mediated cytotoxicity, J. Immunol. 156 (1996) 3678–3686.
[25] A. Weren, B. Bonnekoh, B. Schraven, H. Gollnick, A. Ambach, A novel flow cytometric assay focusing on perforin release mechanisms of cytotoxic T lymphocytes, J. Immunol. Methods 289 (2004) 17–26.
[26] S. Lam, C. Bollard, T-cell therapies for HIV, Immunotherapy 5 (2013) 407–414.
[27] J. Lieberman, P.R. Skolnik, G.R. Parkerson 3rd, J.A. Fabry, B. Landry, J. Bethel, et al., Safety of autologous, ex vivo-expanded human immunodeficiency virus (HIV)-specific cytotoxic T-lymphocyte infusion in HIV-infected patients, Blood 90 (1997) 2196–2206.
[28] L. Shan, K. Deng, N.S. Shroff, C.M. Durand, S.A. Rabi, H.C. Yang, et al., Stimulation of HIV-1-specific cytolytic T lymphocytes facilitates elimination of latent viral reservoir after virus reactivation, Immunity 36 (2012) 491–501.
[29] S.G. Deeks, HIV: shock and kill, Nature 487 (2012) 439–440.
[30] R.B. Jones, S. Mueller, R. O'Connor, K. Rimpel, D.D. Sloan, D. Karel, et al., A subset of latency-reversing agents expose HIV-infected resting CD4+ T-cells to recognition by cytotoxic T-lymphocytes, PLoS Pathog. 12 (2016) e1005545.
[31] M.A. Purbhoo, D.J. Irvine, J.B. Huppa, M.M. Davis, T cell killing does not require the formation of a stable mature immunological synapse, Nat. Immunol. 5 (2004) 524–530.
[32] S.L. Maude, N. Frey, P.A. Shaw, R. Aplenc, D.M. Barrett, N.J. Bunin, et al., Chimeric antigen receptor T cells for sustained remissions in leukemia, N. Engl. J. Med. 371 (2014) 1507–1517.
[33] J.M. Folkvord, C. Armon, E. Connick, Lymphoid follicles are sites of heightened human immunodeficiency virus type 1 (HIV-1) replication and reduced antiretroviral effector mechanisms, AIDS Res. Hum. Retroviruses 21 (2005) 363–370.
[34] Y. Fukazawa, R. Lum, A.A. Okoye, H. Park, K. Matsuda, J.Y. Bae, et al., B cell follicle sanctuary permits persistent productive simian immunodeficiency virus infection in elite controllers, Nat. Med. 21 (2015) 132–139.
[35] E. Connick, T. Mattila, J.M. Folkvord, R. Schlichtemeier, A.L. Meditz, M.G. Ray, et al., CTL fail to accumulate at sites of HIV-1 replication in lymphoid tissue, J. Immunol. 178 (2007) 6975–6983.